

# Pattern scaling based projections for precipitation and potential evapotranspiration: sensitivity to composition of GHGs and aerosols forcing

Yangyang Xu<sup>1</sup>  • Lei Lin<sup>2,3</sup>

Received: 12 May 2016 / Accepted: 11 December 2016 / Published online: 5 January 2017  
© Springer Science+Business Media Dordrecht 2017

**Abstract** Pattern scaling is a computationally efficient method to generate global projections of future climate changes, such as temperature and precipitation, under various emission scenarios. In this study, we apply the pattern-scaling method to project future changes of potential evapotranspiration (PET), a metric highly relevant to hydroclimate research. While doing so, this study tests the basic assumption of pattern-scaling methods, which is that the underlying scaling pattern is largely identical across all emission scenarios. We use a pair of the large-ensemble global climate model (GCM) simulations and obtain the two separate scaling patterns, one due to greenhouse gasses (GHGs) and the other due to aerosols, which show substantial regional differences. We also derive a single combined pattern, encapsulating the effects of both forcings. Using an energy balance climate model, future changes in temperature, precipitation, and PET are projected by combining the separate GHGs and aerosols scaling patterns (“hybrid-pattern” approach) and the performance of this “hybrid-pattern” approach is compared to the conventional approach (“single-pattern”) by evaluating both approaches against the GCM direct output. We find that both approaches provide reasonably good emulations for the long-term projection (end of the twenty-first century). However, the “hybrid-pattern” approach provides better emulations for the near-term climate changes (2020–2040) when the large changes in aerosol emissions occur.

---

**Electronic supplementary material** The online version of this article (doi:10.1007/s10584-016-1879-7) contains supplementary material, which is available to authorized users.

---

✉ Yangyang Xu  
yangyang.xu@tamu.edu

<sup>1</sup> Department of Atmospheric Sciences, Texas A & M University, College Station, TX, USA

<sup>2</sup> School of Atmospheric Sciences, Sun Yat-Sen University, Guangzhou, China

<sup>3</sup> Guangdong Province Key Laboratory for Climate Change and Natural Disaster Studies, Guangdong, China

## 1 Introduction

The pattern-scaling technique is an efficient way to generate future projections of regional climate change under various emission scenarios (Santer et al. 1990; Mitchell 2003). In pattern scaling based climate projections, atmosphere-ocean global climate models (GCMs) are first used to estimate climate change under a specific emission scenario. The time-dependent projection is then separated into time-invariant spatial patterns of certain climate variables normalized by unit temperature change (“scaling pattern”) and the time series of global mean surface air temperature (GMST) change. Simplified climate models, such as energy balance models or intermediate-complexity climate models, are then used to estimate GMST changes under any emission scenarios, a task too expensive for fully coupled 3-dimensional GCMs. Finally, regional climate projections are emulated for a wide range of emission scenarios by multiplying the GMST changes from simple models by the scaling patterns of specific climate variables estimated from the global climate models (e.g., Ishizaki et al. 2014). The pattern-scaling approach has been demonstrated to approximate regional projections of temperature and precipitation satisfactorily for scenarios driven mostly by increases in well-mixed, long-lived greenhouse gas (GHG) concentrations (Mitchell 2003; Tebaldi and Arblaster 2014).

Besides temperature and precipitation, an important climate metric relevant to drought studies is potential evapotranspiration (PET) (Middleton and Thomas 1992). PET is an important component of the Palmer Drought Severity Index (PDSI) (Alley 1984; Dai et al. 2004) and is defined as “the amount of water transpired in unit time by a short green crop, completely covering the ground, of uniform height and never short of water” (Hartmann 1994; Allen et al. 1998). Sherwood and Fu (2014) proposed that the Aridity Index (AI), defined as the ratio of precipitation (P) to PET, should be used for aridity impact studies, rather than precipitation alone, because increases in PET can lead to more severe aridity, even in regions with increasing precipitation (Feng and Fu 2013). Some other studies, alternatively, suggested that PET increase (or AI decrease as in the model projections) may not be very relevant for observed pan evaporation and aridity trends (e.g., Roderick et al. 2015; Milly and Dunne 2016). Nevertheless, PET is a useful metric in that it is an essential input to most local hydrologic (i.e., runoff) impact models and it helps in quantifying irrigation water demand for agriculture activities (Allen et al. 1998).

Using simulations from a GCM, Lin et al. (2015a and b) showed that PET would increase (i.e., drying conditions will become more prevalent) under global warming conditions and the magnitude of drying is larger under higher GHG emissions scenarios. These results are in agreement with earlier work of Feng and Fu (2013) and Scheff and Frierson, (2014). It is unclear, however, whether PET can be reliably obtained using pattern-scaling methods, which is one of the two main objects of this study.

The key assumption of the pattern-scaling approach is that the scaling pattern is not significantly different across emission scenarios (e.g., Representative Concentration Pathway (RCP) emission scenarios, RCP2.6, RCP4.5, RCP6.0, and RCP8.5). Previous research has raised the concern that the scaling pattern for temperature and precipitation could be dependent on how different the sulfate aerosol concentrations are in the emission scenarios (Mitchell et al. 1999; Schlesinger et al. 2000; Mitchell 2003; Shiogama et al. 2009; Ishizaki et al. 2013), but the usefulness of accounting for aerosol differences in the scenarios has not been fully assessed.

Therefore, in addition to providing a pattern scaling based projection of PET, another objective of this study is to examine how the pattern-scaling approach may be sensitive to the

composition of radiative forcing or GMST change (Shiogama et al. 2009; Ishizaki et al. 2013; Tebaldi and Arblaster 2014). In this study, we used two sets of ensemble simulations from a GCM (one under the CMIP5 scenario RCP8.5 and one under the same RCP8.5 GHG emissions but keeping aerosol emissions at 2005 levels), to obtain the normalized spatial pattern of three climate variables (temperature, precipitation, and PET) due to GHGs and aerosols separately. We then multiplied the scaling patterns by the changes in GMST projected by an energy balance climate model to emulate climate change under standard RCP scenarios. The “hybrid-pattern” based projections were evaluated against the direct output of GCMs and were compared to the traditional pattern-scaling approach that used a single pattern.

## 2 Methods

### 2.1 Model description

#### 2.1.1 The global climate model

Community Earth System Model version 1 (CESM1) is a fully coupled ocean–atmosphere–land model that provides state-of-the-art simulations of the Earth’s climate (Hurrell et al. 2013). The horizontal resolution is  $0.9^\circ$  latitude  $\times$   $1.25^\circ$  longitude for the atmospheric component (Community Atmospheric Model 5, CAM5) and  $1^\circ \times 1^\circ$  for the ocean. A comprehensive three-mode modal aerosol module (Liu et al. 2012) and a two-moment bulk cloud microphysical scheme have been implemented (Morrison and Gettelman 2008; Gettelman et al. 2010). CESM1 contains the physics to represent aerosol direct effects, semi-direct effects, and indirect effects for both liquid and ice phase clouds (Ghan et al. 2012), and it can capture the observed geographical and temporal variations of aerosol mass and number concentrations, size distributions, and optical properties (Liu et al. 2012).

### 2.2 The energy balance model (EBM)

The time evolution of GMST across all four RCP scenarios was also calculated using a simple energy balance model as in Ramanathan and Xu (2010). The zero-dimensional EBM has been validated against three-dimensional GCMs (Hu et al. 2013), and Figure S1.a shows the agreement of global average temperature simulated by the EBM and CESM1 (anomaly relative to 2006–2015).

The simple EBM accounts for historical and future variations in the energy input to the climate system attributable to natural factors (solar), GHGs, ozone, and aerosols (i.e., sulfate, nitrates, black carbon, and organic carbon). The total, GHG, and aerosol forcing time series used by the simple model were obtained from the RCP database (Figure S1.b, c, d). The temperature evolution due to GHGs and aerosols can then be calculated separately using the EBM and used in conjunction with the scaling patterns (obtained as described in Section 2.3) to emulate climate change under different emission scenarios.

### 2.3 GCM experiments under four RCP scenarios and a fixed-aerosols scenario

- (1) The CESM1 Large Ensemble (LE) consists of 30-member simulations from 1920 to 2080. The simulation beyond 2005 is forced by RCP8.5. Each member of the

simulations is forced by the same GHG and aerosol forcing trajectory but starts from randomly perturbed initial conditions in the atmosphere (Kay et al. 2015).

- (2) We also performed another set of simulation (15 ensemble members), forced by RCP8.5 except that aerosol precursor emissions and atmospheric oxidants are fixed at the year 2005 level (RCP8.5\_FixA) (Xu et al. 2015).
- (3) The RCP4.5 Medium Ensemble (ME) uses the same strategies to perturb initial conditions as Large Ensemble but with a smaller ensemble size of 15 and is forced by RCP4.5 (Sanderson et al. 2015).
- (4) Three ensemble members of CESM1 under RCP6.0 were performed as part of phase 5 of the Coupled Model Intercomparison Project (CMIP5) (Meehl et al. 2013).
- (5) Three ensemble members of CESM1 under RCP2.6 were performed as part of phase 5 of the Coupled Model Intercomparison Project (CMIP5) (Meehl et al. 2013).

The simulations in (3), (4), and (5) are used as the benchmark for evaluation of the pattern-scaling approach.

## 2.4 Obtaining the scaling patterns

The climate change pattern for a climate variable  $C(x, i)$  as simulated by a GCM at location  $x$  and time  $i$  can be approximated by:

$$C^*(x, i) = T(i) \times p(x) \quad (1)$$

$T(i)$  is the time-dependent scaling factor,  $p(x)$  is the time-invariant scaling pattern, and  $C^*(x, i)$  is the time-dependent pattern emulated by the product of the two terms (Mitchell et al. 1999). The value of  $T(i)$  we used here is, as commonly done in pattern scaling projections, GMST change during the first through the seventh decade of the twenty-first century (the 2010s to 2070s), with the 1985–2005 average used as the baseline. That is  $T(i)$  is a time series of temperature (units: °C), such as 2010–2019 mean minus 1985–2005 mean, 2020–2029 minus 1985–2005, ..., 2070–2079 minus 1985–2005.

$p(x)$  describes how a climate variable changes at location  $x$  when the GMST rises by 1°C and is obtained from the set of regression coefficients that minimize the root-mean-square of the differences between the directly simulated pattern  $C(x, i)$  and the emulated pattern  $C^*(x, i)$ , as follows:

$$p(x) = \frac{\sum_i [T(i) \times C(x, i)]}{\sum_i T(i)^2} \quad (2)$$

Scaling patterns,  $p(x)$ , for most climate variables, are usually expressed as the percentage change per °C of global warming with respect to the baseline. Previous research has often obtained  $p(x)$  based on a single, multi-forcing emission scenario (e.g., RCP8.5 or RCP4.5, see Fig. 1a, b), or as the average of individual patterns derived from different emission scenarios (Tebaldi and Arblaster 2014). Our study, in contrast, aimed at distinguishing the spatial patterns of climate response to GHGs (P\_GHG, Fig. 1c) and aerosols forcings (P\_aerosol, Fig. 1d) separately.

Firstly, we used the ensemble simulation with fixed aerosols (RCP8.5\_FixA) to obtain the scaling pattern due to GHGs forcing only (P\_GHG, Fig. 1c). For example, to get the scaling pattern for precipitation, we applied the regression method as described above using precipitation and temperature changes from RCP8.5\_FixA. Secondly, we contrasted

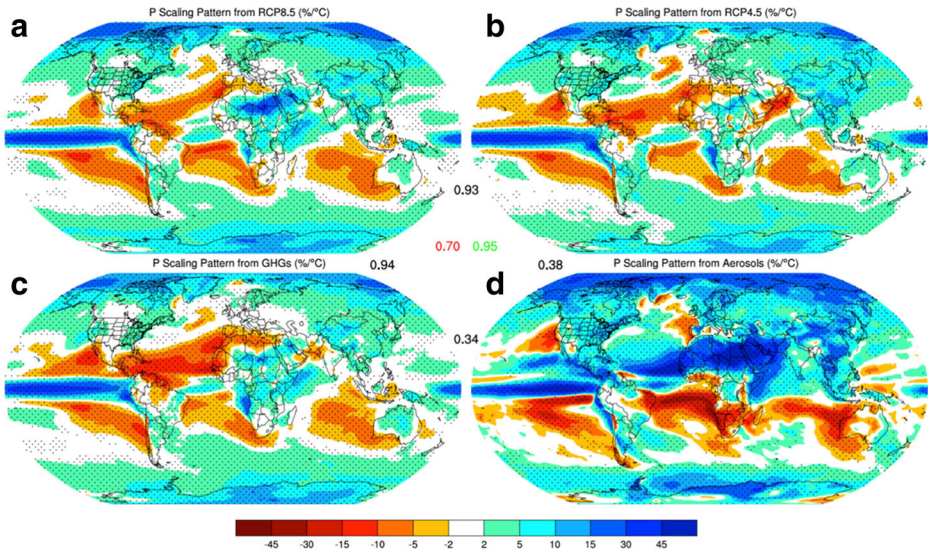


**Fig. 1** The scaling patterns of annual mean precipitation changes (%/°C) in response to changes in RCP8.5 (a), RCP4.5 (b), and GHGs only (c), aerosols only (d). Patterns a and b are used for the “single-pattern” approach for projection, while c and d are used for the “hybrid-pattern” approach. Note that “GHGs only” (c) and “aerosol only” (d) scaling patterns are obtained from RCP8.5 and RCP8.5\_FixA simulations. The *four black numbers* next to adjacent maps show the pattern correlation between the two maps. The *red number* (0.70) shows the pattern correlation between the panels a and d. The *green number* (0.95) shows the pattern correlation between the panels b and c. Note the remarkable distinction between c and d and the similarity between a and b. The *dotted regions* have significant changes in precipitation across ensemble members (i.e., more than 80% of simulations have the same sign of changes). A similar figure with the absolute precipitation changes (mm/day/°C) is shown in Figure S2

RCP8.5 and RCP8.5\_FixA for every decade of twenty-first century (2010s to 2070s) to obtain the temperature and precipitation due to aerosol only (RCP8.5–RCP8.5\_FixA), assuming linear additivity of the two responses, and then calculated the scaling pattern due to anthropogenic aerosols forcing only (P\_aerosols, Fig. 1d). Some non-linearity when adding different responses are expected (Ming and Ramaswamy 2009), but our previous work using the same model and different aerosol forcing (Xu et al. 2016) suggested that the responses to individual forcing are linearly additive (e.g., for the warming vertical profile of temperature change).

## 2.5 Two approaches of pattern scaling projections: hybrid-pattern and single-pattern

Using a simple energy balance model (Ramanathan and Xu 2010) and the separate radiative forcing of GHGs and aerosols (van Vuuren et al. 2011, shown in Figure S1.c and d), we can calculate the contribution of GHGs and aerosols to GMST change separately ( $\Delta T_{\text{GHGs}}$  and  $\Delta T_{\text{aerosols}}$ ).

For the “hybrid-pattern” approach, the spatial distributions of climate change can be obtained by combining both  $\Delta T_{\text{GHGs}} \times P_{\text{GHGs}}$  (Fig. 1c) and  $\Delta T_{\text{aerosols}} \times P_{\text{aerosols}}$  (Fig. 1d). Alternatively, we also emulated the climate change projection by calculating  $\Delta T_{\text{All}} \times P_{\text{RCP8.5}}$  (Fig. 1a), which is the conventional “single-pattern” approach. The

performance of both approaches can be evaluated against the direct model output from the same climate model, both regarding pattern correlation and absolute errors (root mean square of errors, RMSE). The evaluation results are shown in Section 3.2.

### 3 Results

#### 3.1 Scaling patterns due to GHGs vs. aerosols

The ensemble mean scaling patterns for the percentile change of precipitation derived from RCP4.5 and RCP8.5, using the traditional, single-pattern approach, are shown in Fig. 1a, b. Over most of the globe, especially in the high latitude regions where the internal variability of rainfall is smaller, precipitation changes are significant (dotted regions in Fig. 1), satisfying the test that at least 80% of ensemble members show the same sign of change (Feng and Fu 2013).

The precipitation change pattern is characterized by a tropical oceanic rainfall enhancement and subtropical rainfall suppression, although considerable differences exist at the regional scale (e.g., North Africa, Arabian Sea). It is unclear why the relative precipitation changes are larger over Sahara regions in RCP8.5 ( $>40\%/^{\circ}\text{C}$ ) than those in RCP4.5 (other studies have found larger changes under RCP2.6, Tebaldi and Arblaster 2014). This prominent difference could be simply due to the extremely dry base climate (as a close-to-zero denominator for the percent change). Indeed, we note that the absolute change (mm/day/ $^{\circ}\text{C}$ ) over this dry region is not significantly larger in RCP4.5 (Figure S2).

The high similarity between RCP8.5 (Fig. 1a) and RCP4.5 (Fig. 1b), with the pattern correlation coefficient at 0.93, supports the notion of adopting a single scaling pattern across scenarios. Even when computing the pattern correlation coefficient using all data points rather than only those with significant changes, its value remains as high as 0.90. In contrast, the scaling patterns due to GHGs only (Fig. 1c) and aerosols only (Fig. 1d) are remarkably different, with a low pattern correlation coefficient at 0.34 (or 0.32 if calculated using all data points). Changes with opposite signs occur in many places (northern South America, northern and southern Africa, and Australia). The most notable difference is the northward shift of tropical rainfall in the aerosol case. The physical mechanisms of precipitation change due to GHG changes have been discussed by many previous studies (Allen and Ingram 2002; Held and Soden 2006; Richter and Xie 2008). The spatial heterogeneity of precipitation response to aerosols arises from the asymmetric nature of the forcing that is stronger over Northern Hemisphere (Chung and Seinfeld 2005; Shindell et al. 2012; Hwang et al. 2013; Ocko et al. 2014). Note that the normalized process in Fig. 1 effectively reversed the sign of aerosol cooling so that the Northern Hemisphere features a stronger warming. The pattern correlations between patterns due to GHGs only (Fig. 1c) and those obtained from RCP8.5/RCP4.5 (Fig. 1a, b) are also high (0.94–0.95), because both RCP8.5 and RCP4.5 scenarios are primarily driven by GHG changes, as we will examine closely later.

Figure 2 shows the scaling patterns of PET over land from the different scenarios. The pattern correlation between the patterns derived from GHGs and RCP8.5/RCP4.5 is high (0.99/0.98). In these three scaling patterns, relative PET increases in high latitudes more than low latitudes (as found in Scheff and Frierson, 2014; Fu and Feng 2014; Lin et al. 2015a). But the scaling pattern in response to aerosols forcing (Fig. 2d) shows larger changes in South America, Europe, North Africa, and East Asia, with a weak decrease in

India and most of sub-Sahara Africa. The pattern correlation between GHGs and aerosols is 0.90–0.92. The warmer temperature in response to higher GHG levels tends to increase PET due to the larger vapor pressure deficit and also the change in Clausius–Clapeyron slope (Scheff and Frierson, 2014). In contrast, aerosols can impact PET strongly through reducing net shortwave radiation reaching the surface in addition to the temperature effect (Lin et al. 2015b). Indeed, the scaling patterns for surface air temperature are similar to those for PET in the GHG case (Figure S3.c), but less so in the aerosol case (Figure S3.d). All pattern correlations among GHGs, RCP4.5, and RCP8.5 are above 0.96, while these patterns are relatively distinct from the aerosol pattern (pattern correlations: 0.85–0.92), which features much stronger changes over Northern Hemispheric land.

From Figs. 1 and 2, the pattern obtained from only one emission scenario (“single-pattern” approach) has mixed influences of both GHGs and aerosols, but with predominant contributions from GHGs. This implies that a “single-pattern” approach can be applicable when the global mean aerosol loading changes are small. On the other side, a “single-pattern” approach would be problematic if aerosols lead to considerable forcing contribution in future climate change. Next, we examine the usefulness of combining GHGs and aerosols scaling patterns (“hybrid-pattern” approach) in emulating future climate projections, which has been suggested by the previous studies (Mitchell et al. 1999; Ishizaki et al. 2014).

### 3.2 Evaluating the pattern scaling projection: hybrid- vs. single-pattern approach

Figure 3a shows the CESM1 projected change pattern in precipitation for 2040–2049 relative to the baseline (1985–2005) under RCP4.5, as the reference for evaluating two pattern scaling projection approaches. Note that the changes are scaled by global mean

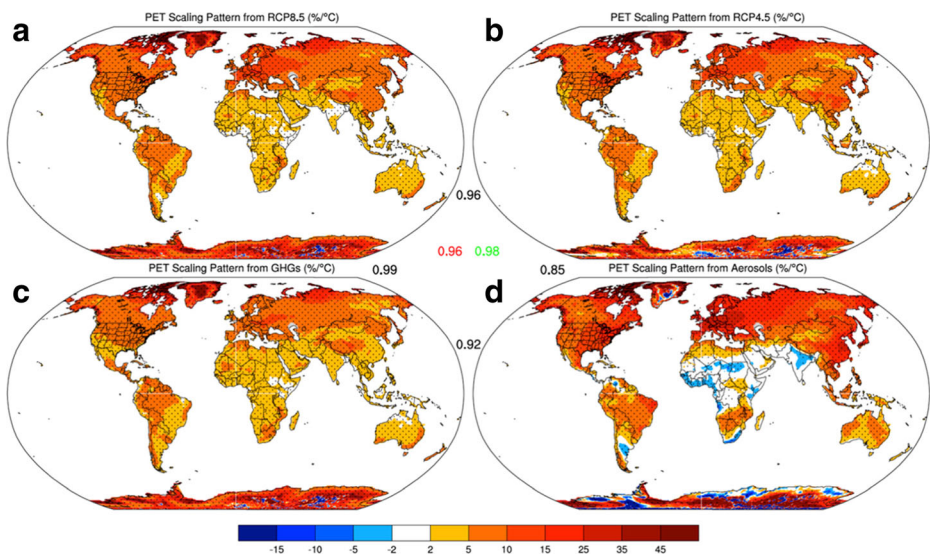


**Fig. 2** The same as Fig. 1 except for PET over land. The scaling pattern for temperature is similar (Figure S3) because the temperature is a dominating factor for PET along with surface radiation budget. Note “GHGs only” (c) and “aerosol only” (d) scaling patterns are obtained from RCP8.5 and RCP8.5\_FixA simulations

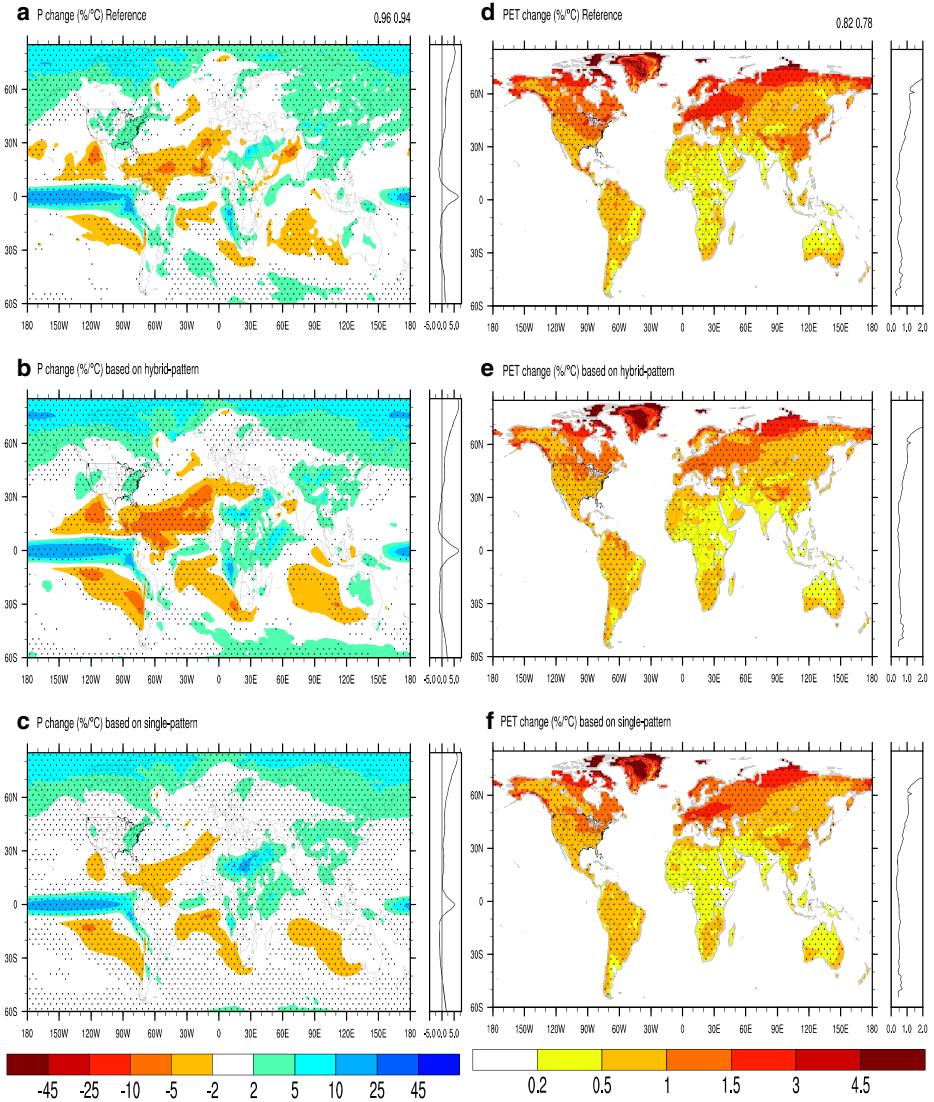


**Fig. 3** (Left) Projected changes in precipitation (%/°C) at 2040s relative to 1985–2005 under RCP4.5, with the zonal average shown on the right-hand side of the map. **a** CESM1 direct output as the “Reference” for the evaluation. **b** Projection using the “hybrid-pattern” approach. **c** Projection using the “single-pattern” approach. All values were normalized by the change of GMST during this period (about 1.3°C). The two numbers at the top right showed the pattern correlation between **a** and **b** and between **a** and **c**. The significance of changes was assessed using the same method as in Figs. 1 and 2. (Right) Same as the left, except for PET over land. The pattern correlation of PET maps seems lower (0.82/0.78) because they are calculated only using values over major land regions (–60°S–85°N), while the pattern correlation of *P* on the left (0.96/0.94) are based on global values. If *P* pattern correlation were calculated only using land regions, they would also be lower (0.86/0.82)

temperature change during this period (1.3°C) to focus on the spatial pattern. The pattern correlation between CESM1 direct output and “hybrid-pattern” approach (Fig. 3b) is 0.96, higher than that between CESM1 and “single-pattern” approach (Fig. 3c, 0.94). Notably,



there was a drying band (reduction in the zonal average of precipitation) around 10°N–30°N in the RCP4.5 simulations, which was well captured in the “hybrid-pattern” approach, but this feature was largely missing in the “single-pattern” approach (see the zonal average plot in Fig. 3c). Similar results are also found if the absolute changes of precipitation (mm/day) are considered (Figure S4.c).

For PET, the “hybrid-pattern” approach also demonstrated a better performance in emulating mid-century changes than the “single-pattern” approach (0.82 and 0.78 in pattern correlations, respectively). However, the “hybrid-pattern” approach underestimated the projected PET increase in Europe compared to the “single-pattern” approach (Fig. 3d–f).

Note that the procedure of significance test is affected by the internal variability (i.e., model ensemble spread) at the regional scale. Consequently, Fig. 3c (“single-pattern” approach) appears to have more dotted regions on it, because “single-pattern” approach used all 30 ensemble members of RCP8.5 simulations (Kay et al. 2015), and the internal variability is suppressed to a greater extent than those in Fig. 3b (using 15 available ensemble members of RCP8.5-FixAerosol as in Xu et al. (2015)) and Fig. 3a (using 15 ensemble members as in Sanderson et al. (2015)).

As for the changes throughout the twenty-first century, with the GHG forcing growing with time, the pattern of external responses increasingly overwhelms the effects of internal variability, which lead to the pattern correlations of both two methods approaching to unity at the end of twenty-first century (Figure S5, left). The main reason that the correlations increase with time and the RMSE decrease with time is that the signal-to-noise ratio becomes higher (Mitchell et al. 1999).

The benefit of using the “hybrid-pattern” approach is quantitatively examined next. Firstly, the pattern correlation (Figure S5, left) and the globally averaged RMSE (Figure S5, right) of temperature, precipitation, and PET between the two pattern scaling approaches and the direct model output for RCP4.5, RCP6.0, and RCP2.6 were calculated. Note that PET is only calculated over the land. Thus, it has smaller pattern correlation and larger RMSE compared to precipitation, due to a larger variability over the land. Secondly, the ratios of the “hybrid-pattern” approach and “single-pattern” approach are shown in Fig. 4, the projected patterns from the “hybrid-pattern” approach are overall better than the “single pattern” approach, indicated by a larger-than-one ratio for pattern correlation and smaller-than-one ratio for RMSE. The difference between the two approaches in the near-term (the 2020s, 2030s, and 2040s) is larger when the aerosol forcing makes a considerable fraction of the total forcing (Figure S1.e). The ratio approaches unity in the late twenty-first century, which implies that the “single-pattern” approach is more suitable for the long-term climate projection when changes are dominated by GHG effects.

The emulated results using the “hybrid-pattern” approach for RCP2.6 are not always better than those under RCP4.5 or RCP6.0, as one may expect from the fact that the aerosol forcing is relatively larger in RCP2.6 (Figure S1.e). This is probably because only three ensemble members were available for RCP2.6 and RCP6.0 as the benchmark, which is more subject to the influence of internal variability. This larger influence for small ensemble in RCP2.6 and RCP6.0 can be readily seen from the larger decadal fluctuation of blue and green lines in Fig. 4 (and Figure S5), as opposed to the rather monotonic trends of RCP4.5 (black lines).

In summary, although the “single-pattern” approach demonstrates slightly lower RMSE in precipitation (Figure S5.d), the “hybrid-pattern” approach performs better in obtaining the zonally averaged change (Fig. 3). The “single-pattern” approach can be appropriately

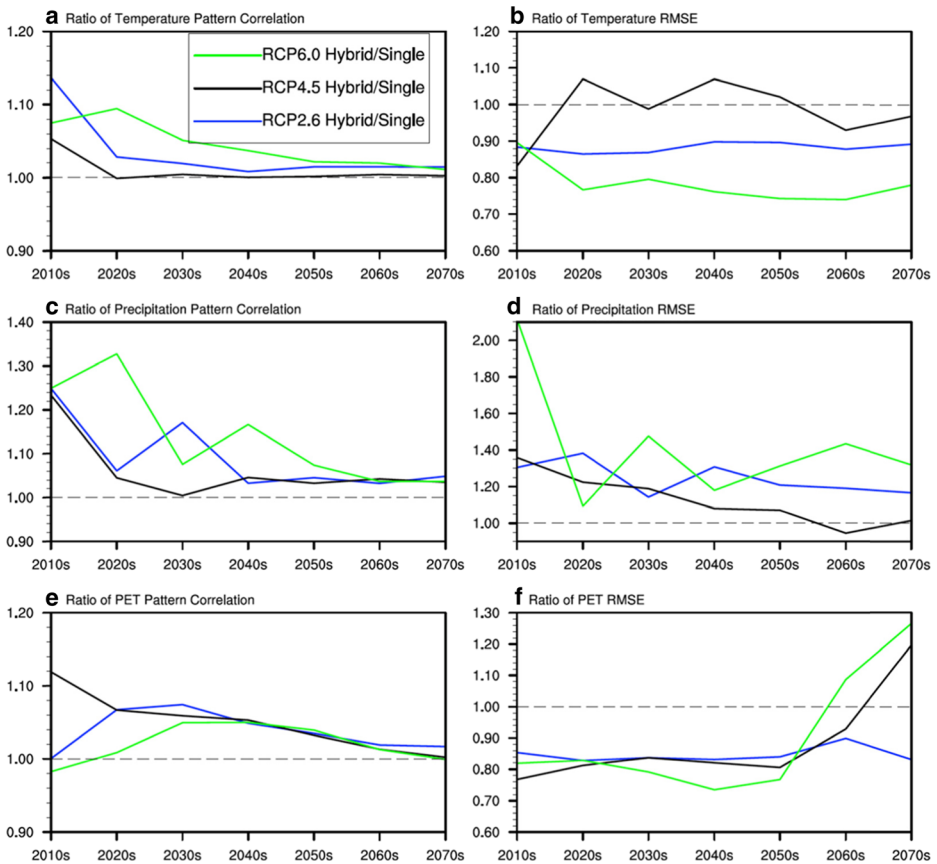


**Fig. 4** (Left) The ratio of “hybrid-pattern” approach and “single-pattern” approach, in the centered pattern correlation between each pattern-scaling approach and the direct GCM output (Figure S5). The larger-than-one ratio indicates a better performance of “hybrid-pattern” approach. Top row: temperature; middle row: precipitation; and bottom row: PET. (Right) Same as the Left but for globally averaged RMSE. The smaller-than-one ratio indicates a better performance of “hybrid-pattern” approach

used to project the long-term changes under standard RCPs since all these scenarios assume a sharp decrease in aerosol emission toward the end of the century. But the “single-pattern” approach may be biased in scenarios with a significant difference in the composition make-up (ratio of GHG vs. aerosol forcing). These scenarios include the near-term climate projection for the twenty-first century as we discussed here, but would also be the relevant ones in geoengineering studies that consider different methods (e.g., carbon capture vs. solar radiation management; Tilmes et al. 2016).

## 4 Concluding remarks

The first objective of this study was to utilize a pattern-scaling approach for future projection of PET, which is not discussed in the previous literature. This approach was shown to produce reasonably good emulations of GCM projection, as expected, considering that PET changes are governed by temperature changes to a large extent.

This study also aimed at characterizing the robustness of pattern-scaling methods in the presence of aerosol forcing, thus addressing one of the challenges that pattern-scaling methods are commonly thought of facing, i.e., the characterization of a signal from scenarios containing significant sources of spatially non-homogenous forcings. Using a pair of CESM1 simulations under RCP8.5 scenarios with and without aerosol changes, we separately obtained the scaling patterns of temperature, precipitation, and PET due to GHGs and aerosols. We used those two patterns simultaneously with GMST changes from a simple energy balance model to emulate future changes of temperature, precipitation, and PET in three other RCP scenarios. Our approach used a large ensemble (15 to 30 members) as opposed to some earlier studies (e.g., three ensemble members in Ishizaki et al. 2013). The scaling pattern is obtained based on regression of each ensemble members, despite that all results are presented as the ensemble average. The variability between ensemble members are often at the regional (sub-continental) scale, and thus, the pattern correlation is high between ensemble members. This ensemble spread due to natural variability is utilized to provide statistical significance test, which allows us to better identify the signal of forced change.

We found that considering the influence of aerosols separately increases the pattern correlation in temperature, precipitation, and PET and decreases the global RMSE in temperature and PET, hence, justifying the usefulness of a “hybrid-pattern” approach. The assumption that the scaling pattern remains stable across all emission scenarios (“single-pattern” approach) cannot be reliably applied if the change of aerosol forcing is large, for example, in the next few decades as expected. For regional climate change at the end of twenty-first century, however, the “single-pattern” approach provides reasonably good emulation, because aerosol influence gradually diminishes through the century and becomes negligible by its end. Of course, the benefit of adopting a “hybrid-pattern” approach comes at the cost of conducting additional GCM simulations to obtain GHG and aerosol patterns separately. On this note, presumably, an even more accurate (but also more computationally expensive) approach is to separate the climate change response pattern due to aerosol emissions from individual continents (e.g., Europe vs. Asia), as proposed by Hulme et al. (2000).

Note that due to internal variability, the obtained response pattern to GHG and aerosol forcing can vary greatly from model to model. Therefore, one caveat of the current analysis is that we only used a single set of parameters in the EBM (fitted to a single climate model, Figure S1), and this approach failed to account for the model uncertainty in the climate sensitivity and potentially regional pattern. We are now working to improve this aspect by including CMIP5 model output into a future pattern-scaling analysis on extreme weather events, with the problem being that not many of them provide aerosol forcing-only simulations. Given the increasing availability of computational resources, the model dependence of aerosol-induced climate responses should be further tested within a multi-model framework, to examine whether the findings of this study are robust.

**Acknowledgements** We thank Andrew Gettelman and Claudia Tebaldi for comments on an earlier draft. We thank two anonymous reviewers for careful review and constructive comments. Y. Xu acknowledges supports from US Department of Energy’s Office of Science (BER, DE-FC02-97ER62402) and Advanced Study Programme (ASP) postdoctoral fellowship while he worked at NCAR. L. Lin is supported by the National Basic Research Program of China (2016YFA0602700) and National Natural Science Foundation of China (41330527). Computing resources were provided by the Climate Simulation Laboratory at NCAR’s Computational and Information Systems Laboratory, sponsored by the National Science Foundation and other agencies. The National Center for Atmospheric Research is supported by the US National Science Foundation.

## References

- Allen MR, Ingram WJ (2002) Constraints on future changes in climate and the hydrologic cycle. *Nature* 419:224–232
- Allen RG, Pereira LS, Raes D, Smith M (1998) Crop evapotranspiration-guidelines for computing crop water requirements-FAO irrigation and drainage paper 56, vol 300. FAO, Rome, p 6541
- Alley WM (1984) The palmer drought severity index: limitations and assumptions. *J Clim Appl Meteorol* 23: 1100–1109. doi:10.1175/1520-0450(1984)023<1100:TPDSIL>2.0.CO;2
- Chung S, Seinfeld J (2005) Climate response of direct radiative forcing of anthropogenic black carbon. *J Geophys Res* 110:1–25. doi:10.1029/2004JD005441
- Dai A, Trenberth KE, Qian T (2004) A global dataset of palmer drought severity index for 1870–2002: relationship with soil moisture and effects of surface warming. *J Hydrometeorol* 5:1117–1130. doi:10.1175/JHM-386.1
- Feng S, Fu Q (2013) Expansion of global drylands under a warming climate. *Atmos Chem Phys* 13:10081–10094. doi:10.5194/acp-13-10081-2013
- Fu Q, Feng S (2014) Responses of terrestrial aridity to global warming. *J Geophys Res B Solid Earth* 119:7863–7875. doi:10.1002/2014JD021608
- Gottelman A, Liu X, Ghan SJ et al (2010) Global simulations of ice nucleation and ice supersaturation with an improved cloud scheme in the community atmosphere model. *J Geophys Res Atmos* 115:D18216. doi:10.1029/2009JD013797
- Ghan SJ, Liu X, Easter RC et al (2012) Toward a minimal representation of aerosols in climate models: comparative decomposition of aerosol direct, semidirect, and indirect radiative forcing. *J Clim* 25:6461–6476. doi:10.1175/JCLI-D-11-00650.1
- Hartmann D (1994) *Global Physical Climatology*. Academic Press, San Diego, pp 411
- Held IM, Soden BJ (2006) Robust responses of the hydrological cycle to global warming. *J Clim* 19:5686–5699. doi:10.1175/JCLI3990.1
- Hu A, Xu Y, Tebaldi C et al (2013) Mitigation of short-lived climate pollutants slows sea-level rise. *Nat Clim Chang* 3:730–734. doi:10.1038/nclimate1869
- Hulme M, Wigley TML, Barrow EM et al (2000) Using a climate scenario generator for vulnerability and adaptation assessments: MAGICC and SCENGEN version 2.4 workbook. Climatic Research Unit, Norwich, p 60
- Hurrell JW, Holland MM, Gent PR et al (2013) The community earth system model: a framework for collaborative research. *Bull Am Meteorol Soc* 94:1339–1360. doi:10.1175/BAMS-D-12-00121.1
- Hwang YT, Frierson DMW, Kang SM (2013) Anthropogenic sulfate aerosol and the southward shift of tropical precipitation in the late 20th century. *Geophys Res Lett* 40:2845–2850. doi:10.1002/grl.50502
- Ishizaki Y, Yokohata T, Emori S et al (2013) Validation of a pattern scaling approach for determining the maximum available renewable freshwater resource. *J Hydrometeorol* 15:505–516. doi:10.1175/JHM-D-12-0114.1
- Ishizaki Y, Shiogama H, Emori S et al (2014) Dependence of precipitation scaling patterns on emission scenarios for representative concentration pathways. *J Clim* 26:8868–8879. doi:10.1175/JCLI-D-12-00540.1
- Kay JE, Deser C, Phillips A et al (2015) The Community Earth System Model (CESM) large ensemble project: a community resource for studying climate change in the presence of internal climate variability. *Bull Am Meteorol Soc* 96:1333–1349. doi:10.1175/BAMS-D-13-00255.1
- Lin L, Gottelman A, Feng S, Fu Q (2015) Simulated climatology and evolution of aridity in the 21st century. *J Geophys Res Atmos*. 120:2014JD022912. doi: 10.1002/2014JD022912
- Lin L, Gottelman A, Fu Q, Xu Y (2015) Simulated differences in 21st century aridity due to different scenarios of greenhouse gases and aerosols. *Clim Change*. 1–16. doi: 10.1007/s10584-016-1615-3
- Liu X, Easter RC, Ghan SJ et al (2012) Toward a minimal representation of aerosols in climate models: description and evaluation in the community atmosphere model CAM5. *Geosci Model Dev* 5:709–739. doi:10.5194/gmd-5-709-2012
- Meehl G, Washington WM, Arblaster JM et al (2013) Climate change projections in CESM1(CAM5) compared to CCSM4. *J Clim* 26:6287–6308. doi:10.1175/JCLI-D-12-00572.1
- Middleton NJ, Thomas DSG (1992) UNEP: world atlas of desertification. Edward Arnold, Sevenoaks
- Milly PCD, Dunne KA (2016) Potential evapotranspiration and continental drying. *Nat Clim Chang* 6:946–949. doi:10.1038/NCLIMATE3046
- Ming Y, Ramaswamy V (2009) Nonlinear climate and hydrological responses to aerosol effects. *J Clim* 22:1329–1339. doi:10.1175/2008JCLI2362.1
- Mitchell TD (2003) Pattern scaling—an examination of the accuracy of the technique for describing future climates. *Clim Change* 60(3):217–242
- Mitchell JFB, Johns TC, Eagles M, Ingram WJ, Davis RA (1999) Towards the construction of climate change scenarios. *Clim Change* 41:547–581

- Morrison H, Gettelman A (2008) A new two-moment bulk stratiform cloud microphysics scheme in the community atmosphere model, version 3 (CAM3). Part I: description and numerical tests. *J Clim* 21: 3642–3659. doi:[10.1175/2008JCLI2105.1](https://doi.org/10.1175/2008JCLI2105.1)
- Ocko IB, Ramaswamy V, Ming Y (2014) Contrasting climate responses to the scattering and absorbing features of anthropogenic aerosol forcings. *J Clim* 27:5329–5345. doi:[10.1175/JCLI-D-13-00401.1](https://doi.org/10.1175/JCLI-D-13-00401.1)
- Ramanathan V, Xu Y (2010) The Copenhagen accord for limiting global warming: criteria, constraints, and available avenues. *Proc Natl Acad Sci U S A* 107:8055–8062. doi:[10.1073/pnas.1002293107](https://doi.org/10.1073/pnas.1002293107)
- Richter I, Xie S-P (2008) Muted precipitation increase in global warming simulations: a surface evaporation perspective. *J Geophys Res Atmos* 113:D24118. doi:[10.1029/2008JD010561](https://doi.org/10.1029/2008JD010561)
- Roderick ML, Greve P, Farquhar GD (2015) On the assessment of aridity with changes in atmospheric CO<sub>2</sub>. *Water Resour Res* 51:5450–5463. doi:[10.1002/2015WR017031](https://doi.org/10.1002/2015WR017031)
- Sanderson BM, Oleson KW, Strand WG, et al. (2015) A new ensemble of GCM simulations to assess avoided impacts in a climate mitigation scenario. *Clim Change*. 1–16. doi: [10.1007/s10584-015-1567-z](https://doi.org/10.1007/s10584-015-1567-z)
- Santer BD, Wigley TML, Schlesinger ME et al (1990) Developing climate scenarios from equilibrium GCM results, technical note 47. Max Planck Institute Meteorologie, Hamburg, p 29
- Scheff J, Frierson DMW (2014) Scaling potential evapotranspiration with greenhouse warming. *J Clim* 27:1539–1558. doi: [10.1175/JCLI-D-13-00233.1](https://doi.org/10.1175/JCLI-D-13-00233.1)
- Schlesinger ME, Malyshev S, Rozanov EV, et al. (2000) Geographical Distributions of Temperature Change for Scenarios of Greenhouse Gas and Sulfur Dioxide Emissions. *Technol Forecast Soc Change* 65:167–193. doi: [http://dx.doi.org/10.1016/S0040-1625\(99\)00114-6](http://dx.doi.org/10.1016/S0040-1625(99)00114-6)
- Sherwood S, Fu Q (2014) A drier future? *Science* (80-) 343(80-):737–739. doi:[10.1126/science.1247620](https://doi.org/10.1126/science.1247620)
- Shindell DT, Voulgarakis A, Faluvegi G, Milly G (2012) Precipitation response to regional radiative forcing. *Atmos Chem Phys* 12:6969–6982. doi:[10.5194/acp-12-6969-2012](https://doi.org/10.5194/acp-12-6969-2012)
- Shiogama H, Emori S, Takahashi K et al (2009) Emission scenario dependency of precipitation on global warming in the MIROC3.2 model. *J Clim* 23:2404–2417. doi:[10.1175/2009JCLI3428.1](https://doi.org/10.1175/2009JCLI3428.1)
- Tebaldi C, Arblaster JM (2014) Pattern scaling: its strengths and limitations, and an update on the latest model simulations. *Clim Change* 122:459–471. doi:[10.1007/s10584-013-1032-9](https://doi.org/10.1007/s10584-013-1032-9)
- Tilmes S, Sanderson BM, O'Neill BC (2016) Climate impacts of geoengineering in a delayed mitigation scenario. *Geophys Res Lett* 43:8222–8229. doi:[10.1002/2016GL070122](https://doi.org/10.1002/2016GL070122)
- van Vuuren DP, Edmonds J, Kainuma M et al (2011) The representative concentration pathways: an overview. *Clim Change* 109:5–31. doi:[10.1007/s10584-011-0148-z](https://doi.org/10.1007/s10584-011-0148-z)
- Xu Y, Lamarque J-F, Sanderson BM (2015) The importance of aerosol scenarios in projections of future heat extremes. *Clim Change*. 1–14. doi: [10.1007/s10584-015-1565-1](https://doi.org/10.1007/s10584-015-1565-1)
- Xu Y, Ramanathan V, Washington WM (2016) Observed high-altitude warming and snow cover retreat over Tibet and the Himalayas enhanced by black carbon aerosols. *Atmos Chem Phys* 16:1303–1315. doi:[10.5194/acp-16-1303-2016](https://doi.org/10.5194/acp-16-1303-2016)